LUND UNIVERSITY

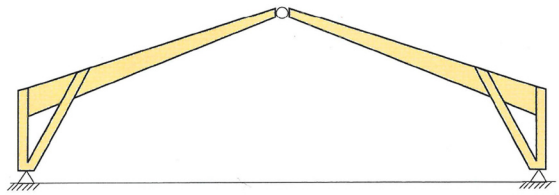

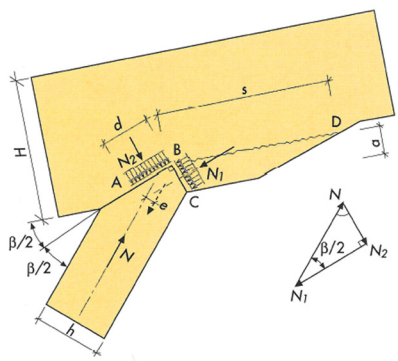

DESIGN METHOD FOR STRUT-BEAM CONNECTION IN HINGED FRAMES

JUAN CARDENAL BASTÉ

Structural Mechanics

Master's Dissertation

Department of Construction Sciences
Structural Mechanics

ISRN LUTVDG/TVSM--12/5150--SE (1-44)
ISSN 0281-6679

DESIGN METHOD FOR STRUT-BEAM CONNECTION IN HINGED FRAMES

Master's Dissertation by

JUAN CARDENAL BASTÉ

Supervisors:
Henrik Danielsson *Lic.Eng.*,
Div. of Structural Mechanics, LTH, Lund

Arne Emilsson,
Limträteknik AB, Falun

Examiner:
Per Johan Gustafsson *Professor*,
Dept. of Construction Sciences, LTH, Lund

Printed by Media-Tryck LU, Lund, Sweden, July, 2012 *(Pl)*.

For information, address:
Division of Structural Mechanics, LTH, Lund University, Box 118, SE-221 00 Lund, Sweden.
Homepage: http://www.byggmek.lth.se

Acknowledgements

The work presented in this master's thesis started in the spring of 2007 and, after several attempts, was completed during the spring of 2012 at the Division of Structural Mechanics at the Lund Institute of Technology in Sweden.

I would therefore like to express my most sincere gratitude to my supervisors Prof. Per Johan Gustaffson and Lic. Eng. Henrik Danielsson for their endless patience and unconditional support during this time. This thesis would have otherwise probably never been concluded.

Abstract

Glulam is almost exclusively the chosen material of timber frame structures. Of those, three-hinged (three-pin) portal frames are incomparably the most common type. Being both statically determinate and stable against horizontal forces in its own plane offer both practical (basic constructive details) and economical benefits.
The design of the haunch allows for various solutions: it can be curved with continuous laminates, finger jointed, jointed with steel dowels and slotted-in plates, or built-up with a strut.
The form of the frame derives from the main load's force line. The most appropriate forms for large spans are curved or built-up haunches, as they fulfil both functional and aesthetic aspects. Three-pin portal frames are suitable for spans up to 30-40 meters, being the limiting factor the transport feasability of the frame's halves.

In recent years a handful of three-hinged structures with built-up haunches have collapsed, leaving behind a need to analyse and study the stresses and resistance of this structures. For obvious reasons it is specially interesting to research and clarify the fracture risk on the built-up haunches as well as to map the stresses created by the inner frame leg through compression to the lower edge of the frame rafter.
Today there is only one general method used to design built-up haunches, present in both the Glulam Handbook and the German Institute for Standardization, DIN, which is based on *established practice*. Both standards share similar simplifications and assumtions, giving surprisingly little importance to the shear stress that occurs in the contact area of the built-up haunch.

The aim of this master's thesis was to put together a tool, in form of a diagram, to help design the built-up haunch, with particular emphasis on the contact area between the inner frame leg and the frame rafter, and the subsequent shear stresses this contact creates on the rafter. To achieve this result a sample frame rafter was calculated using 2D frame software and generic loads and materials. The section forces obtained were then used to create a FEM model of the built-up haunch.
This FEM model provided a clearer understanding of the behaviour of the frame leg-frame rafter's contact area as well as yielding a map of the shear stresses present in the joint. Finally with the use of Linear Elastic Fracture Mechanics and the mean stress criterion a diagram-tool was created.

This report yielded two results that may be deemed of special interest:

- both the Glulam Handbook and the german DIN standard relegate the shear stress in the notch as merely a design checkout, never a design factor.
- Both the Glulam Handbook and the DIN completely disregard the size effects in the capacity of *birdmouth joints*. The fracture mechanics cal-

culations presented in this report provide prove of strong size effects, so that current design standards significantly overestimate the capacity of great-sized built-up haunches.

This conclusion could be important in practical terms, and should be further investigated. Experimental tests should also be inlcuded in future research.

Keywords: glulam, built-up haunches, framed joint, three-pin portal frames, shear stress, failure modes, LEFM, ABAQUS, size effects.

Sammanfattning

Limträ är nästan uteslutande det valda trämaterialet i större ramkonstruktioner. Av dessa är treledsramar ojämförligt den vanligaste typen. Att vara både statiskt bestämd och stabil mot horisontella krafter i sitt eget plan ger både praktiska (enklare konstruktiva detaljer) och ekonomiska fördelar. Ramhörnen kan utformas på olika sätt: det kan vara krökta, fingerskarvade, skruvade eller sammansatta med en tryckspräva eller ett inre ramben. Ramens form bör om möjligt följa huvudlastens trycklinje. De mest lämpliga former för stora spännvidder är böjda eller sammansatta, då de uppfyller både funktionella och estetiska krav. Treledsrammar är lämpliga för spännvidder upp till 30-40 meter, den begränsande faktorn är transport av ramens halvor.

Ett antal konstruktioner av denna typ har emellertid kollapsat under senare år. Det finns därför ett behov av att analysera spänningar och bärförmåga. I detta arbete ägnas särskilt intresse åt spänningar och risk för brott i anslutning mellan tryckspräva och balk i ett ramörn.

För närvarande finns det bara en allmän metod som används för att dimensionera sammansatta ramhörn. Den bygger på gammal praxis och utgör grunden både för dimensioneringsmetod angiven i Limträhandboken och för en likartad metod angiven i tyska DIN. Båda anvisningarna har liknande förenklingar och antaganden, vilket ger förvånansvärt liten inverkan på beräknad skjuvspänning i det kritiska området.

Syftet med detta examensarbete var att sätta ihop ett verktyg, i form av ett diagram, för att hjälpa dimensionera sammansatta hörn med särskild tonvikt på skjuvspänningar som uppstår i rambalken invid anliggningsytan mellan en tryckspräva och rambalken. Detta resultat nåddes genom ramberäkning med hjälp av ett 2D ramanalys datorprogram för bestämning av normalkrafter, tvärkrafter och moment. Snittkrafterna som erhölls från denna beräkningen användes sedan för att göra finita elementberäkningar för analys av spänningar och brott i ramhörnet.
Slutligen, och med hjälp av linjärelastisk brottmekanik och ett medelspänningskriterium skapades ett diagramverktyg.

Examensarbetet gav även två slutsatser som kan bedömas vara av särskilt intresse:

- Både Limträhandboken och tyska DIN hanterar skjuvspänningen i anslutningen mellan tryckspräVan och balk enbart som en dimensioneringskontroll, aldrig som en dimensionerande faktor.
- Både Limträhandboken och DIN bortser helt från storlekseffekter i bärförmå gan hos ett sammansatt ramhörn. Brottmekanikberäkningarna redovisade i denna rapport tyder emellertid på en kraftig storlekseffekt, sådan att nuvarande normer kraftigt överskattar bärfärmågan hos ramhörn med stora

dimensioner om normerna ger en rättvisande dimensionering av små eller medelstora ramhörn.
Denna beräkningsslutsats kan vara praktiskt viktig och det kan föreslås att den i framtida forskning bör undersökas experimentellt.

Contents

Chapter 1

Introduction

1.1 Background

Glulam has become a well embraced material being used in many types of construction such as halls, churches, playgrounds, bridges, aviation hangars, electricity masts.... Timber portal frames, almost exclusively executed in glulam, have gained popularity as an economical alternative to steel framed construction used in comercial and industrial buildings [1]. It has become so due to the many advantages glulam offers, namely the possibility of obtaining larger dimensions than structural timber and the fact that the weight/strength ratio is only two thirds of steel and only one sixth of the weight/strength of concrete [5].

The deformation and strength of glulam is affected by the moisture content, its gradients and the duration of the loads. Its extreme anisotropy makes it specially important for the designer to pay attention to connections between components where the train of forces in the framework shift orientation [19]. This is particularly important in supports and *haunches.*

The need to cover large spans (in some cases of up to 50m) and the need to preserve the design both functional and esthetical have entailed the use of *curved* and *built-up haunches* as the most convenient form of structural frame.

Both designs improve the function of the building at the cost of somewhat lower utilization of the material [1]. The fact that these type of structures are hinged at the foundations makes them specially suitable for meager, low quality soils.

One of the main resources engineers and designers possess when facing the

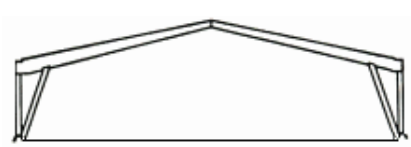

Figure 1.1: Model of a three-pin hinged frame.

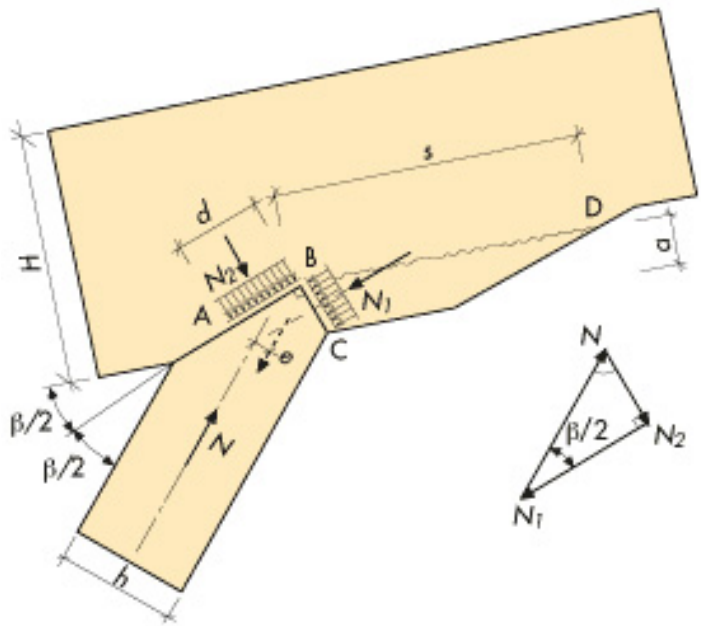

Figure 1.2: Detail of the force distribution of a frame joint.

task of calculating a glulam structure is the *Glulam Handbook*, distributed by the Swedish Timber industry, commonly used as a guide for both pre and final design.

It is in portal frames, specially in its *three-pin* version, where the importance of well thought–off haunches and supports emerge as crucial elements in the design of a successful construction.

It is specifically here, in the 9th chapter, when covering the design of haunches for built–up portal frames, where the aforementioned handbook acknowledges a shortcoming in its guidance by stating:

> *The distribution of forces in this well-tried form of connection is* unclear *but according to established practice...*

1.2 Objectives

The purpose of this thesis is, essentially, to:

- Lay out the distribution of shear stresses in the frame joint between the frame rafter and the frame legs through contact pressure.
- Create a graphic tool that provides the engineers and designers with a substantially less empirical instrument of designing frame joints in built–up haunches.

The present study relates to the strength of the type of joint shown in figure 1.2

1.3 Limitations

Beyond the inevitable limitation of time, this report is confined in the context of short-term loads at constant environmental conditions. Therefore, the all-important time-dependent effects of transient moisture conditions, creep fracture (strength reduction of long duration loads), and eigenstresses have been consciously overlooked. As is usual in timber engineering strength design, timber will be regarded as a statistically homogeneous material.

Chapter 2

Shear stress distribution. An example of a frame joint

2.1 Frame Analysis

A calculation of a three-hinge frame was carried out with Strusoft's WIN-Statiks Ramanalys ver. 5.3.002. This software is ideal for analyzing plane structures with arbitrary geometry and according to the 1st and 2nd order theory.

2.1.1 Geometry

The chosen frame for calculation is shown in figure 2.1 with the dimensions defined in table 2.1. The frame has a total span of 50m and a maximum height of 10.7m. The roof pitch is 15 degrees. The building is 84m long (15 frames at c/c between frames being the usual 6m).

Table 2.1: Frame geometry

Hall length	L	84 m
Hall span (width)	W	50 m
Ridge height	H	10.7 m
Column height	h	4.0 m
Roof pitch (alpha)	α	15°
Distance between frames	c/c	6.0 m
Angle between frame rafter and strut (beta)	β	39°
Inclination of the strut (delta)	δ	54°

Sections used

The sections chosen for this calculation are 1620x215 mm^2 for the frame rafters, 405x215 mm^2 for the struts and 270x215 mm^2 for the columns.

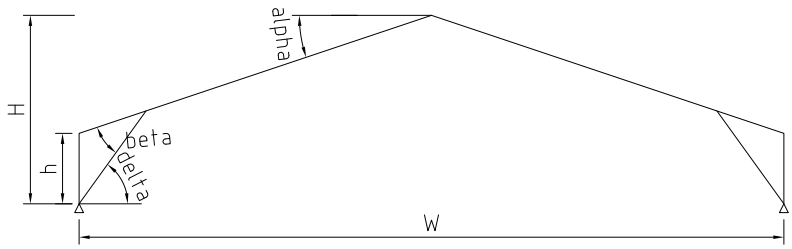

Figure 2.1: Frame parameters

2.1.2 Loads

There are usually 3 types of loads that can act on a portal frame:

1. *Deadweight roof*, see figure 2.2

$$G_{k,roof} = 0.45 \text{ kN/m}^2$$

expressed as a line load (kN/m):

$$g_{k,roof} = 0.45 \times (c/c) = 0.45 \times 6 \text{ m} = 2.7 \text{ kN/m}$$

This load includes the usual roofing materials set above the frame such as purlins and load-bearing roof sheets.

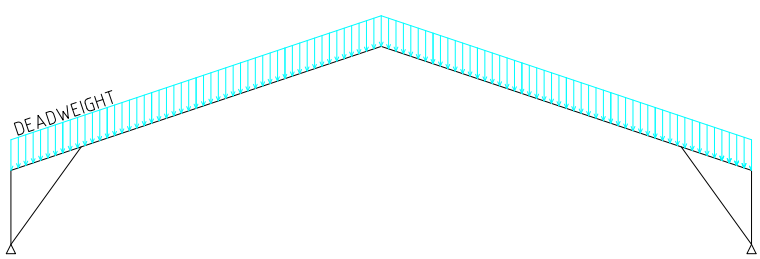

Figure 2.2: Distribution of the roof's deadweight

The deadweight of the structural elements in the frame is automatically linked to the loadcase *Deadweight roof* in Ramanalys.

2. *Snow load*, see figure 2.3

   The snow load base value is a geography-dependent value. In this case a moderate to high value was chosen:

$$s_o = 2.5 \text{ kN/m}^2$$

   The load reduction factor $\psi \leqslant 1$ depends on the type of load and its variation in time as well as the load's statistical variability.
   A time-variable load, for which high values occur rarely and with a short duration, is therefore defined by a low value of ψ.
   The usual load value, ψQ_k, is used when variable loads are combined. Normally there is only one load with characteristic value in a loadcombination, the *principal value*, while the remaining loads have usual values.

   In this case, the load reduction factor for the snow load is presented in table 2.2.

Table 2.2: Load reduction factor for snow load.(BKR, [3])

Snowload base value, s_o	Load reduction factor ψ
2.5	0.7

   The *Snow and wind load handbook* [2] presents a figure to obtain idealized *form factors* for snow loads depending on the type of roof and its pitch, α.

   In this case, gable roof with $\alpha = 15°$, the following factors were obtained:

$$\mu_1 = \mu_2 = 0.8$$

   The characteristic value for the snow load will then be:

$$s_{k1,2} = \mu s_o = 0.8 \times 2.5 = 2.0 \text{ kN/m}^2$$

   expressed as a line load (kN/m):

$$s_{k1,2} = 2.0 \times (c/c) = 2.0 \times 6 \ m = 12.0 \text{ kN/m}$$

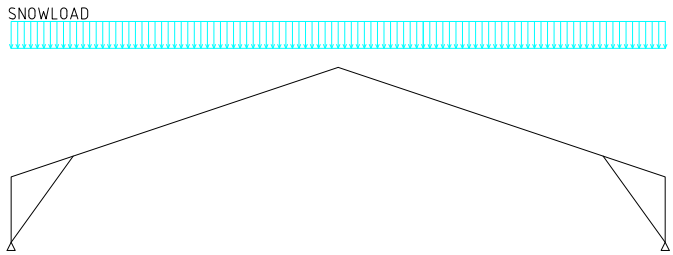

Figure 2.3: Distribution of snow load over the frame

3. *Wind load*, see figure 2.4

A $v_{ref} = 25$ m/s and $h = 10.7$ m yield the following windload pressure:

$$q_k = 0.65 \text{ kN/m}^2$$

Using the diagram for *form factors* of walls and roofs found on [2] the following values were obtained:

- Wind on walls: using $\frac{h}{w} = \frac{10,7}{84} = 0,13$
  - windward: $\mu_{pressure} = 0,85$

    $$q_{k,pressure} = 0.65 \times 0.85 = 0.55 \text{ kN/m}^2$$

    expressed as a line load:

    $$q_{k,pressure} = 0.55 \times 6 \ m = 3.32 \text{ kN/m}$$

  - leeward: $\mu_{draw} = 0,27$

    $$q_{k,draw} = 0.65 \times 0.27 = 0.17 \text{ kN/m}^2$$

    expressed as a line load:

    $$q_{k,draw} = 0.17 \times 6 \text{ m} = 1.05 \text{ kN/m}$$

- Wind on roof:
  - windward, zone C ([1]): $\mu_{draw} = 0,2$

    $$q_{k,draw} = 0.65 \times 0.2 = 0.13 \text{ kN/m}^2$$

    expressed as a line load:

    $$q_{k,draw} = 0.13 \times 6 \text{ m} = 0.8 \text{ kN/m}$$

[1] The effect of zones A and B is neglected for simplicity.

– leeward, zone E ([2]): $\mu_{draw} = 0,40$

$$q_{k,draw} = 0.65 \times 0.40 = 0.26 \text{ kN/m}^2$$

expressed as a line load:

$$q_{k,draw} = 0.26 \times 6 \text{ m} = 1.6 \text{ kN/m}$$

The load reduction factor for windload, according to [3], is ψ=0.25.

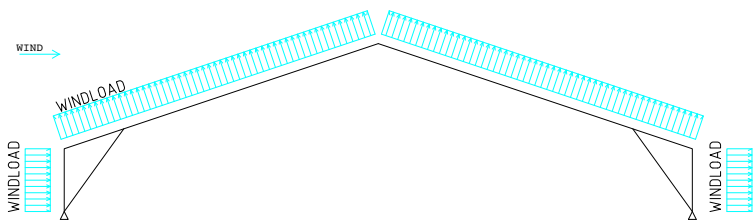

Figure 2.4: Distribution of wind load on the frame

2.1.3 Load combinations

In this case, and according to the swedish general advice and regulations, [3], the most unfavourable combinations for the *ultimate limit state* (ULS) are:

Table 2.3: Load combinations, ULS.

LC	Permanent load	Main variable load	Secondary variable load
1	$1.0G_k$	$1.3W_k$	$1.0\psi S_k$
2	$1.0G_k$	$1.3S_k$	$1.0\psi W_k$

[2]The effect of zone D is neglected for simplicity.

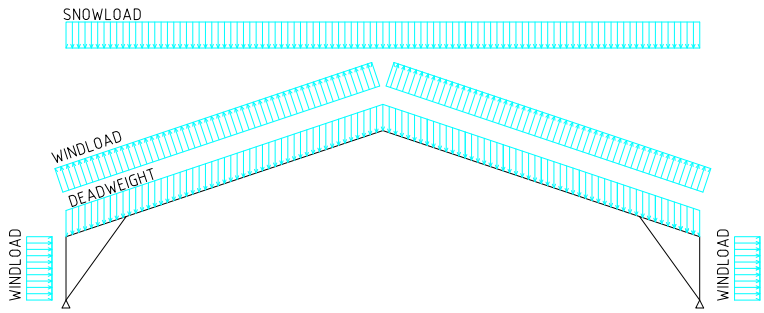

Figure 2.5: Distribution of loads on the frame

2.1.4 Frame analysis method

The frame was analysed as a plane frame (2D) using 1st order theory.

The modulus of elasitcity was set to 10400 MPa. This value is however of minor importance since it does not affect the stress distribution.

Frame geometry and loads are indicated in sections 2.1.1 and 2.1.2 respectively.

Ramanalys works by dividing the frame into members and joints. The joints are those points where the members are connected. As an example, element 2 in figure 2.6 is defined by nodes b and c, where node c is common to elements 2, 3 and 7.

The frame object of the present study is hinged at the notch and at both connections to the ground (strut-column connection), nodes a, c, d, e and g in figure 2.6.

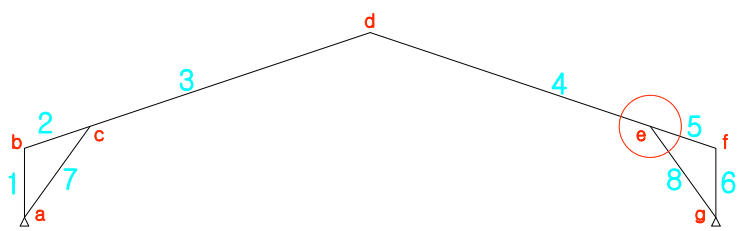

Figure 2.6: Support and joint conditions.

2.1.5 Frame analys section force results

Once all the input data was defined in Ramanalys, the computer calculation took only seconds to complete. Out of the results obtained are in particular the cross-sectional forces and moments acting in the vicinity of the strut-beam

joints of particular interest as a starting point for the subsequent detailed analys of the stresses in the joint. The sectional forces are shown in figure 2.7 and their values presented in table 2.4.

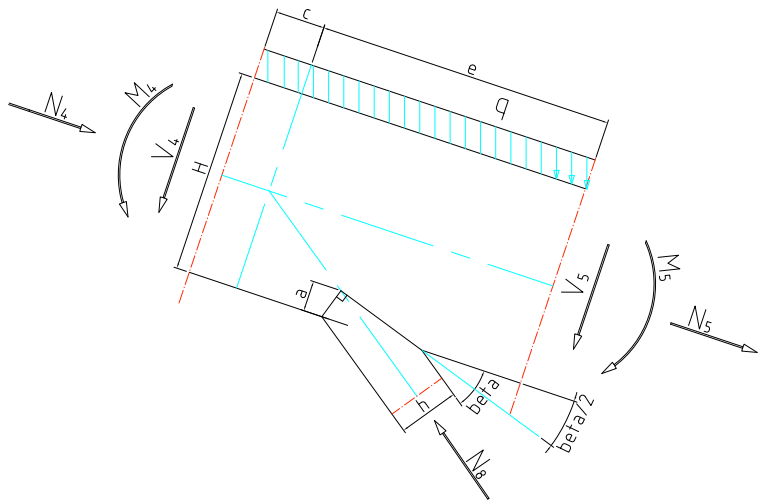

Figure 2.7: Cross-sectional forces and moments.

Table 2.4: Cross-sectional froces and moments.

Element	M (kNm)	V (kN)	N (kN)
4	541.294	239.713	672.527
5	473.489	294.865	76.706
8	0.787	0.481	995.691

2.2 Joint stress analys

The notch was modelled with continuum three-dimensional 8-node brick elements (C3D8R) in ABAQUS. The material was made orthotropic, and its values are resumed in table 2.5.

The loads applied to the model are the ones described in table 2.4.

The *strut*, element 8 in figure 2.7, was replaced wtih two compression loads on the lower edge of the frame rafter.

The subscripts in table 2.5 refer to the main directions in a tree stem, as seen in figure 2.8. The first letter corresponds to the shear component and the second one to the perpendicular direction to the load in the observed plane.

Table 2.5: Material stiffness parameters

	Parameter	Value
Stiffness	E_L	12000 MPa
	E_R	400 MPa
	E_T	400 MPa
	G_{RL}	750 MPa
	G_{TL}	750 MPa
	G_{TR}	75 MPa
Poisson	ν_{RL}	$0,02$
	ν_{TL}	$0,02$
	ν_{TR}	$0,03$

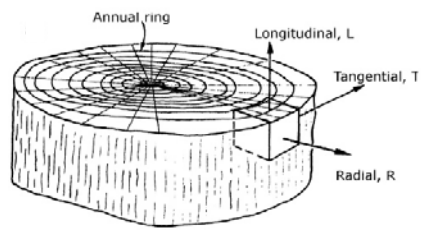

Figure 2.8: Main directions in tree stem.

In order to prevent rigid body displacements 6 degrees of freedom were assigned zero displacement, see figure 2.9. Node number 1 was constrained for displacement in x,y and z directions, number 2 was constrained in y and z directions while node number 3 was constrained in the z direction only.

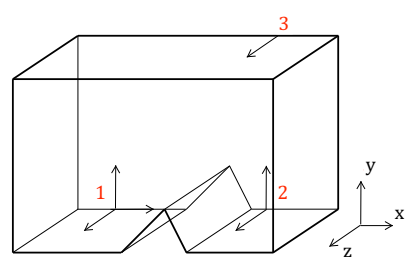

Figure 2.9: Boundary conditions.

The model was meshed as seen in figure 2.10 by partitioning the beam in three general areas to achieve a favourable mesh with fine elements around the notch and coarser elements in the rest of the geometry. The two surfaces that compose the notch had its vertices divided (*seeded* in ABAQUS terms) by about

100 elements each, resulting in an element length of about 6 mm for vertex 1 and 2 mm for vertex 2. In this part a free meshing technique with advancing front was used. On the rest of the vertices a structured meshing was applied and each side was divided by about 70 elements.
In depth (z value in figure 2.9) the vertices were set to an element length of about 40 mm.

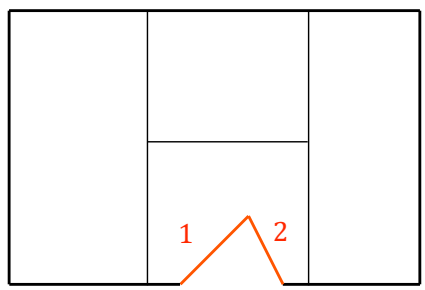

Figure 2.10: Symbolic mesh partitioning.

After *modelling* (creating the geometry, defining the materials, defining boundary conditions, incorporating the cross-sectional loads) and *meshing* the notch had the following appearance:

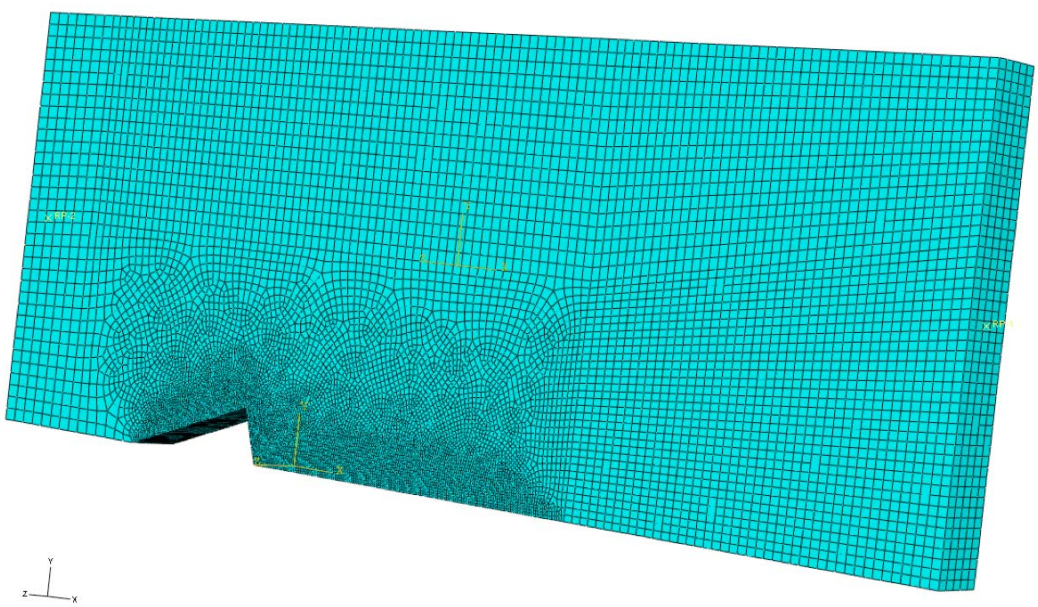

Figure 2.11: Meshed notch in Abaqus.

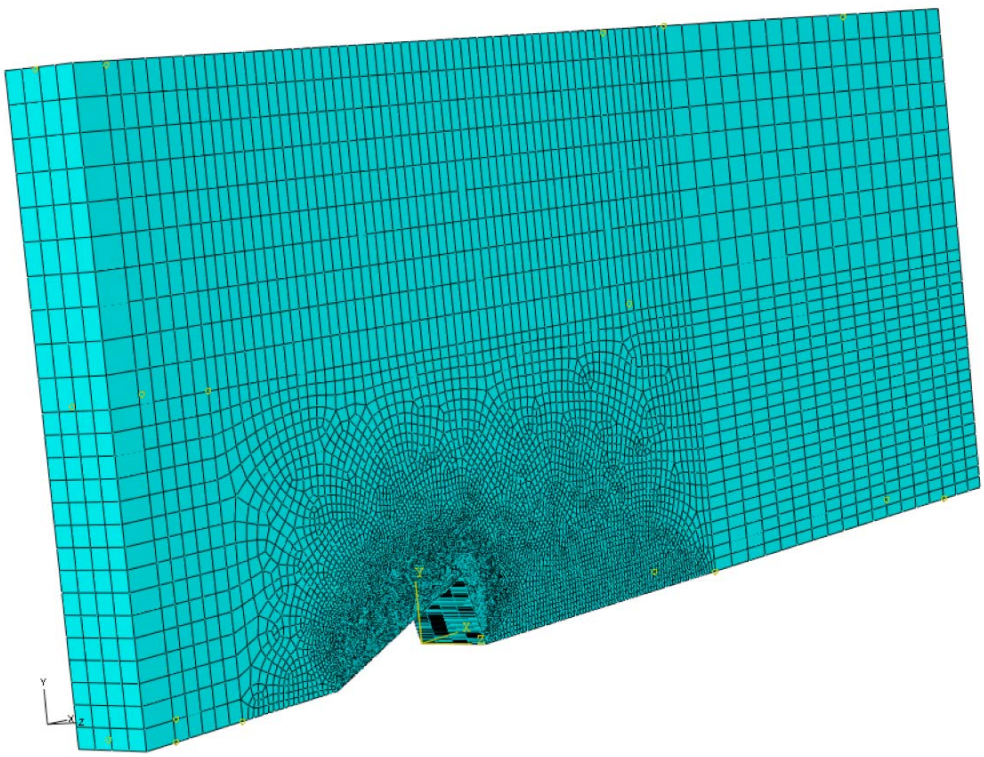

Figure 2.12: Meshed notch. Alternative view.

The next move in the process was to create a calculation and *visualize* the results.

The distribution of the longitudinal shear stress τ_{xy} distribution beginning at the notch and along the frame rafter can be clearly seen in figure 2.13.

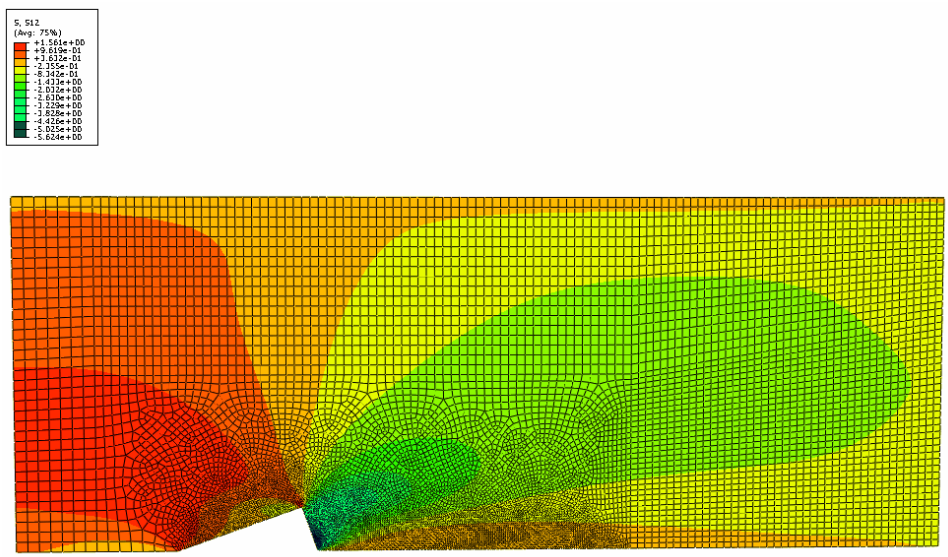

Figure 2.13: Shear stress (τ_{xy}) layout on the notch.

The interesting part of the result resides in the imaginary line, parallel to the edge of the frame raft, located near the edge of the notch.
With the help of MATLAB a series of coordinates were created to extract stress values along that imaginary line. The shear stress is constant along the z-direction (see figure 2.9).

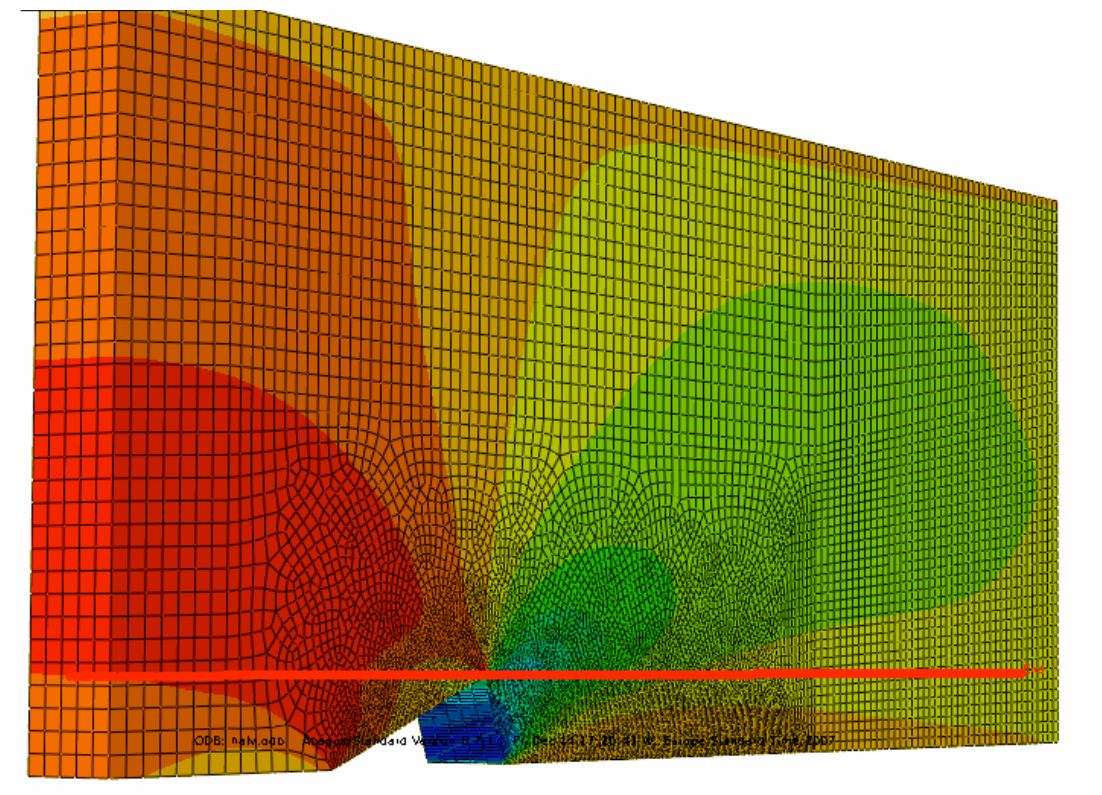

Figure 2.14: Shear stress path.

Those resulting values can be easily assessed in a simple graph[3] as follows:

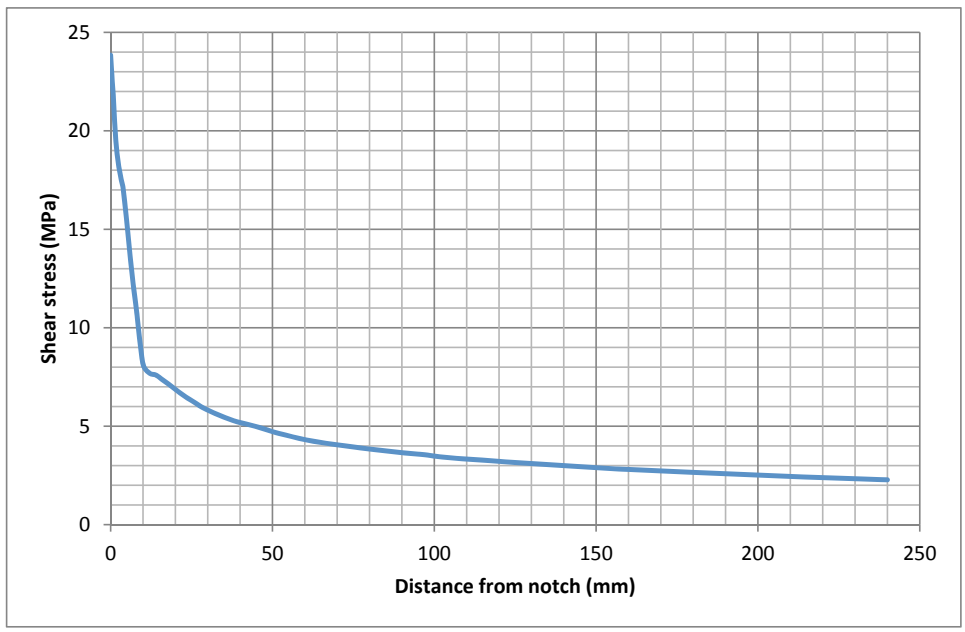

Figure 2.15: Shear stress path from notch.

[3]The graph shows only the part of the path exposed to shear.

Chapter 3

Fracture mechanics predictions of joint strength

3.1 Model for strength prediction: mean stress analysis

3.1.1 Fracture mechanics

The shear force capacity of the frame rafter can be calculated with different methods based on fracture mechanics.

One of the more general methods based on Linear Elastic Fracture mechanics (LEFM) is the *mean stress criterion*. This method allows the possibility of studying the influence that the material's strength, stiffness and fracture energy have on the shear capacity of the beam[6].

Instead of focusing on the stress in a point the mean stress failure criterion considers the mean stress acting across an area of a certain length. The size of the area is governed by the properties of the material[4]. In this study the fracture is assumed to develop along the grain and as a result of shear along the grain.
The failure mode is thus of type II; a sliding (in-plane shear) mode where the crack surfaces slide over one another in a direction perpendicular to the leading edge of the crack, see figure 3.1. The normal stress across the crack is compressive and assumed not to affect the load capacity. This is a, more or less, conservative assumption.

3.1.2 The mean stress approach

With the mean stress approach the mean stress over a certain length is used to calculate the failure load, P_f. According to this method, crack growth will occur when the mean stress, τ_{mean}, equals the shear strength of the material, f_v.[4]

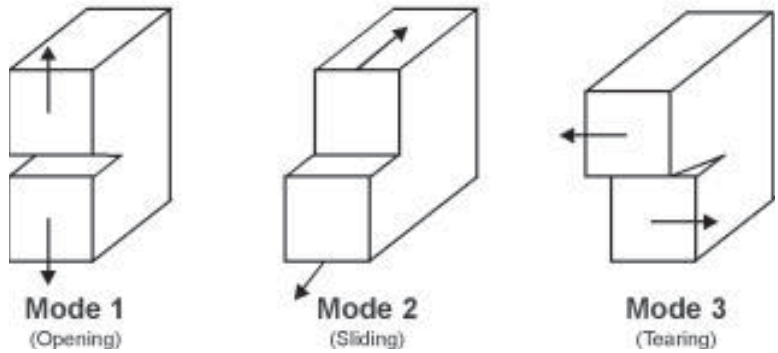

Figure 3.1: Types of failure mode

Due to the fact that the mean stress over a distance is less than the maximum stress over the same distance, the mean stress approach predicts a failure load equal to or larger than the failure load predicted by other conventional stress criteria based on maximum stress in a point. The mean stress method is more general and can be used for structures both with and without a notch or a crack. This method has the advantage that, compared to conventional LEFM approaches, no crack needs to be modeled.

The failure mode II stress intensity factor is defined by:

$$K_{II} = \lim_{r \to 0} \tau_{xy}(r)\sqrt{2\pi r} \qquad \text{for } \theta = 0 \tag{3.1}$$

where r is the distance from the crack tip and θ is the angle with respect to the plane of the crack, as seen in figure 3.2.

The strain energy release rate, G, for a crack under mode II loading is related to the stress intensity factor by:

$$G = \frac{K_{II}^2}{E_{II}} \tag{3.2}$$

where E_{II} is a measure of the isotropic or orthotropic stiffness of the material under consideration. Equation 3.2 is valid for an orthotropic, homogeneous and linear elastic material.

The conventional stress criteria can not be used if there is a crack or notch since the stress theoretically is infinite at the tip of a crack or notch.

The applicability of conventional LEFM is also limited since it can only be used if there is a crack with theoretically infinite stress.

Linear elastic theory predicts that the stress distribution near the crack tip, has the form:

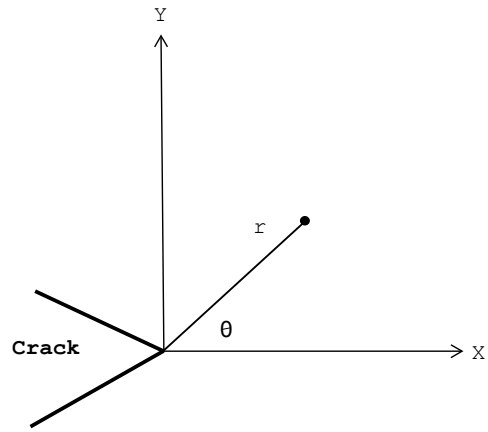

Figure 3.2: Polar coordinates at the crack tip

$$\tau_{xy}(x) = \frac{K_{II}}{\sqrt{2\pi x}} + ... \tag{3.3}$$

where the first term in the series is dominating for small values of x. Assuming only small values of x and using the notation x_o for the length of which the mean stress is calculated, the following expression for mean stress can be obtained:

$$\tau_{mean} = \frac{\int_0^{x_o} \tau(x)dx}{x_o} = \sqrt{\frac{2K_{II}^2}{\pi x_o}} \tag{3.4}$$

By equaling this mean stress to the material's shear strength and incorporating equation 3.2 to equation 3.4, the length over which the mean stress will be calculated is:

$$x_o = \frac{2}{\pi}\frac{E_{II}G_{IIc}}{f_v^2} \tag{3.5}$$

where E_{II} is the effective stiffness for an orthotropic material when loaded in mode 2, and can be calculated according to:

$$E_{II} = \frac{\sqrt{2}E_x}{\sqrt{\sqrt{\frac{E_x}{E_y}} - v_{xy} + \frac{E_x}{2G_{xy}}}} \tag{3.6}$$

The mean stress is calculated for some magnitude P of the load. The *failure magnitude* of the load is then calculated as follows:

$$P_f = \frac{f_v P}{\tau_{mean}} \tag{3.7}$$

3.1.3 Materials

The material property parameter values for glulam used throughout this chapter are taken from [4].

The shear strength is $f_v = 3f_{t,\perp}$ where $f_{t,\perp} = 3.0$ MPa.
The Young's modulus or material stiffness in the direction along the fibres is $E_\parallel = 12000$ MPa, and $E_\perp = \frac{E_\parallel}{30} = 400$ MPa perpendicular to the fibres.
The shear modulus $G_\parallel = \frac{E_\parallel}{16} = 750$ MPa

The fracture energy for failure mode II is $G_{IIC} = 3.5G_{IC}$, where G_{IC} is the fracture energy for failure mode I: $G_{IC} = 300$ J/m^2 (0.3 Nmm/mm^2).

The material properties used in the calculations in this study are summarized in table 3.1.

Table 3.1: Material property parameters

	Parameter	Value
Shear strength	f_v	9.0 MPa
Stiffness	$E_\parallel$	12000 MPa
	$E_\perp$	400 MPa
	$G_\parallel$	750 MPa
Fracture energy	G_{IC}	300 J/m^2
	G_{IIC}	1050 J/m^2

3.1.4 Methodology

Using the equation 3.5 with the parameters defined in table 3.1 the length x_o over which to calculate the mean stress can be computed:

$$x_o = \frac{2}{\pi}\frac{E_{II}G_{IIc}}{f_v^2} = \frac{2}{\pi}\frac{12000 \cdot 1050 \cdot 10^{-3}}{9^2} = 99 \text{ mm} \tag{3.8}$$

The mean stress value along x_o was determined by first integrating the values of τ, obtained in chapter 2 section 2.2, over the distance x_o from the edge of the notch and then dividing the result with the same value, as described in equation 3.9.

$$\tau_{mean} = \frac{\int_0^{x_o} \tau(x)dx}{x_o} \tag{3.9}$$

The mean stress is employed to compute the failure load P_f, as described in equation 3.7.

Finally a curve for the studied geometry can be plotted with the values along the X-axis being defined by H/x_o and those in the Y-axis being defined by P_f/baf_v, where H and b are the height and width of the frame rafter and a the depth of the notch as defined in figure 2.7. The value of P is the value of N_8 as described in figure 2.7 and found in table 2.4.

3.2 Calculation results

Six different geometries were studied. The original geometry, used in chapter 2, is the source for the rest of geometries, which where obtained through different ratios of parameters a and H, both described in figure 2.7.
For each geometry the failure load P_f was calculated for various values of x_o. The geometries analysed can be seen in table 3.2, the failure loads obtained for different values of x_o (99 mm, 940 mm and 1931 mm) are shown in table 3.3. The results are shown graphically in a non-dimensional manner in figure 3.3 as P_f/baf_v versus H/x_o.

Table 3.2: Geometries and corresponding P_f values for x_o=99mm.

Name	H (mm)	a (mm)	a/H	P_f (kN)
0,5H	810	202,5	0,25	1880
0,75H	1215	202,5	0,17	1505
H	1620	202,5	0,13	1380
1,5H	2430	202,5	0,08	1109
2H	3240	202,5	0,06	1034
3H	4860	202,5	0,04	996

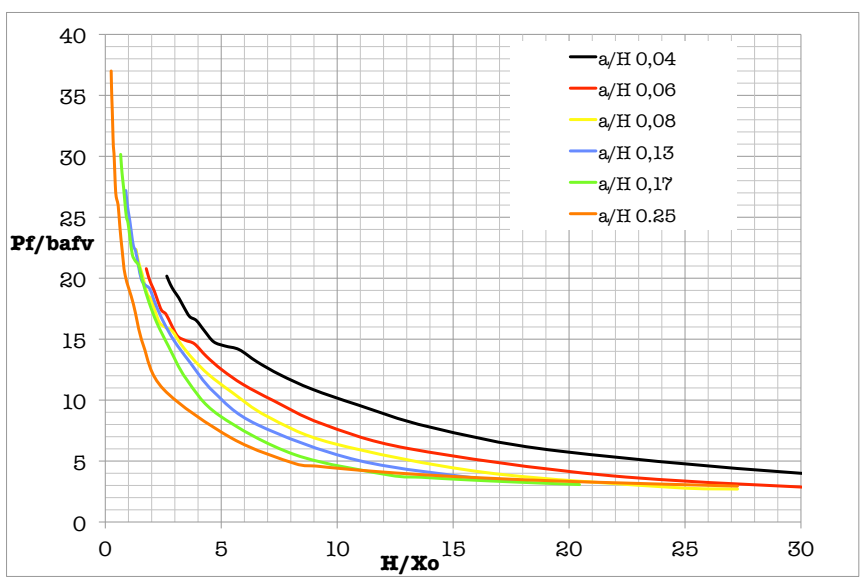

Figure 3.3: Resulting comparative curves for different notch geometries

Table 3.3: Points in the graph for various x_o values.

Name	x_{o1}(99 mm)		x_{o2}(940 mm)		x_{o3}(1931 mm)	
	$P_f/\mathrm{ab}f_v$	H/x_o	$P_f/\mathrm{ab}f_v$	H/x_o	$P_f/\mathrm{ab}f_v$	H/x_o
0,5H	4,8	8,2	20,2	0,9	28,0	0,4
0,75H	3,8	12,3	21,4	1,3	29,4	0,6
H	3,5	16,4	19,4	1,7	26,5	0,8
1,5H	2,8	24,5	15,9	2,6	21,7	1,3
2H	2,64	32,7	14,9	3,4	20,2	1,7
3H	2,5	49,1	14,4	5,2	19,6	2,5

Chapter 4

Comparison of various strength analysis methods

4.1 Joint geometries studied

The original geometry used in this report is the source of the rest of geometries used throughout the present chapter.
The first row in table 4.1 shows the values of the original geometry, each parameter represented in figure 4.1.
The remaining rows are variations of the parameter a in order to produce new geometries through new ratios of a/H.
The angle between the *strut* and the *beam*, β, remains unchanged.

Table 4.1: Studied geometries

a (mm)	H (mm)	β (°)
405	1620	39
270	1620	39
202.5	1620	39
135	1620	39
101.2	1620	39
67.5	1620	39

4.1.1 Joint strength according to Glulam Handbook

According to the The Glulam Handbook [1] the strut is designed as a column, and as such, subject to compression, and normally also to bending [1]. The connection between the frame rafter and the strut is intended to transfer the

[1]The strut is hinged at both ends, but a moment can appear as a result of eccentric loading.

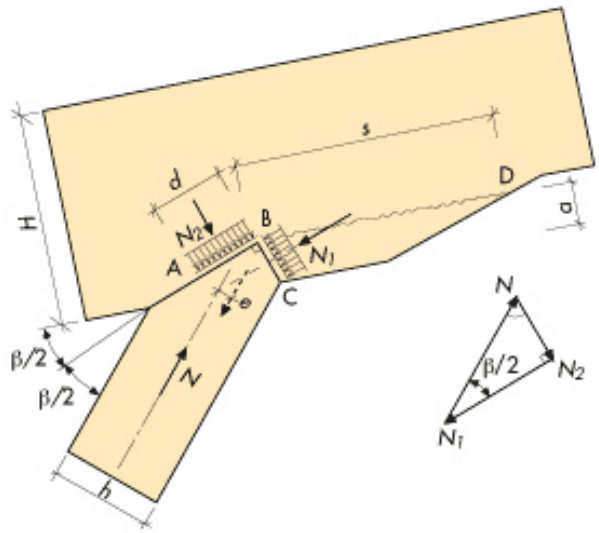

Figure 4.1: Forces in a framed joint.[1]

compression forces principally at the lower edge of the frame rafter through contact pressure.

The strut's compression force, N, is divided in two components, N_1 and N_2, both perpendicular to their respective areas of contact, as shown in figure 4.1. N_1 is assumed to be uniformly distributed across the area BC [1]. The depth of the notch is defined by the parameter a as seen in figure 4.1 and is determined by the following equation:

$$\sigma_{c,\alpha,1} = \frac{N_1}{ba}\cos(\beta/2) \leqslant f_{c,\alpha,1} \tag{4.1}$$

The value of the strength $f_{c,\alpha,1}$ is defined by:

$$f_{c,\alpha} = \frac{f_{c,0}}{\frac{f_{c,0}}{f_{c,90}}\sin^2\alpha + \cos^2\alpha} \tag{4.2}$$

where α is the angle between the direction of the force and the direction of the grain.

The second component of the strut's force, N_2, is assumed to be evenly distributed across an area AB. The required size of this area, bd, is determined by the following condition:

$$\sigma_{c,\alpha,2} = \frac{N_2}{bd} = f_{c,\alpha,2} \tag{4.3}$$

The shear stress at the notch, acting along the line BD, is checked by:

$$\tau = \frac{N_1 \cos(\beta/2)}{bs} \leq f_v \tag{4.4}$$

The length s over which the shear stress is distributed along the frame rafter is confined between the following two values:

$$200mm \leqslant s < 8a$$

A design with a distance BD, as in figure 4.1, less than 200 mm is not allowed. Furthermore, there is a limitation to the depth of the notch, a:

$$a \leqslant \frac{H}{6} \qquad \text{for angles of } \beta \geqslant 60$$

Finally, the cross-sectional size of the strut is checked with:

$$h \geq [a \cdot \tan(\beta/2) + d \cdot \cos(\beta/2)] \cdot \sin\beta \tag{4.5}$$

which is a geometrical control, in that what is checked is that the triangle AB-BC-AC is feasible. The summation of the projected lengths of BC (a) and AB (d) must be less or equal than the length of AC (h), see figure 4.1.

Method

In this case, and in order to find a failure value P_f for the various geometries defined in section 4.1 , the calculation was initiated with the values for geometry of the notch, namely H, h, β and a.

The strength values used for this calculation are taken from the Swedish construction recommendation, BKR (BFS 1993:58), chapter 5:2 table 5:23b. The compression strength parallel and perpendicular to grain are $f_{c,0k}$= 36 MPa and $f_{c,90k}$= 8 MPa respectively. The shear strength parallel to the grain is f_{vk}= 4 MPa.
Applying these values to equation 4.2, yields $f_{c,\alpha,1}$=25, 9 MPa ($\alpha = \beta/2$) and $f_{c,\alpha,2}$=8, 8 MPa ($\alpha = 90 - \beta/2$) respectively.

Results

The results of applying the described methodology are presented in table 4.2:

Table 4.2: Failure loads according to Glulam Handbook

Geometry (a/H)	$P_{f,c}$ (kN)	$P_{f,v}$ (kN)
0,25	2538	3136
0.16	1692	2091
0.12	1269	1568
0.08	846	1045
0.06	634	784
0.04	423	523

Where $P_{f,c}$ represents the compression failure value from using equation 4.1. And $P_{f,v}$ is the value for shear failure obtained from equation 4.4.

4.1.2 Joint strength according to Eurocode 5 (EC5)

The technical rules developed by the European Committee for Standardisation that cover the design of timber buildings and civil engineering works, (EC5), do not present a solution for approaching the design of strut-beam connections in hinged frames. On the other hand, the *German Institute for Standardization* (DIN), from which the EC is widely based, presents an approach in the DIN 1052:2004-08.

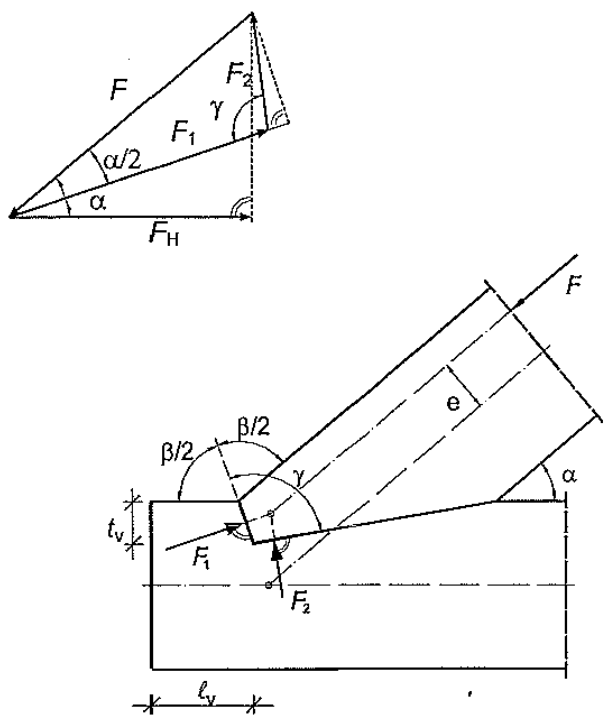

Figure 4.2: Detail and parameters of the notch according to DIN 1052:2004-08

According to the DIN 1052, the depth of the notch, t_v, is chosen depending on the angle of the notch, γ:

$$t_v \leqslant \begin{cases} H/4 & \text{for } \gamma \leqslant 50 \\ H/6 & \text{for } \gamma > 60 \end{cases} \tag{4.6}$$

The design of the joint is acceptable when the compressive stress in the joint

fullfills:

$$\frac{\sigma_{c,\alpha,d}}{f_{c,\alpha,d}} \leqslant 1 \tag{4.7}$$

where

$$\sigma_{c,\alpha,d} = \frac{F_1}{A} \tag{4.8}$$

and

$$f_{c,\alpha,d} = \frac{f_{c,0,d}}{\sqrt{\left(\frac{f_{c,0,d}}{2f_{c,90,d}}\sin^2(\alpha/2)\right)^2 + \left(\frac{f_{c,0,d}}{2f_{v,d}}\sin(\alpha/2)\cos(\alpha/2)\right)^2 + \cos^4(\alpha/2)}} \tag{4.9}$$

A being the projected area defined by:

$$A = b\frac{t_v}{cos(\alpha/2)} \tag{4.10}$$

and F_1 being the component of the compressive force in the strut defined by:

$$F_1 = Fcos(\alpha/2) \tag{4.11}$$

The parameter b in equation 4.10 is the width of the beam and α represents the angle between the strut and the beam.

Combining equations 4.7 and 4.8 with 4.10 and 4.11 yields the following expression:

$$\sigma_{c,\alpha,d} = \frac{Fcos^2(\alpha/2)}{bt_v} \leqslant f_{c,\alpha,d} \tag{4.12}$$

Analogous to the Glulam Handbook, [1], the DIN 1052 suggests checking the shear stress in the joint as:

$$\frac{\tau_{v,d}}{f_{v,d}} \leqslant 1 \tag{4.13}$$

where

$$\tau_{v,d} = \frac{F_H}{l_v b} \tag{4.14}$$

The length over which the shear tension is distributed in the notch, l_v, is limited to:

$$200mm \leqslant l_v < 8t_v$$

and F_H is the horisontal component of the compressive force in the strut, (see figure 4.2):

$$F_H = Fcos(\alpha) \tag{4.15}$$

Combining equations 4.13 with 4.14 and 4.15 results in the following equation:

$$\tau_{v,d} = \frac{Fcos(\alpha)}{l_v b} \leqslant f_{v,d} \tag{4.16}$$

Method

Similar to section 4.1.1, the calculation was initiated with the values for geometry of the notch, namely H, h, α and tv.

The strength values used for this calculation are, as before, taken from the Swedish construction recommendation, BKR (BFS 1993:58), chapter 5:2 table 5:23b. The compression strength parallel and perpendicular to grain are $f_{c,0k}$= 36 MPa and $f_{c,90k}$= 8 MPa respectively. The shear strength parallel to the grain is f_{vk}= 4 MPa.

Applying these values to equation 4.9, yields $f_{c,\alpha,1}$=21, 3MPa.

Results

Applying the above values to the equations described at the beginning of this section yield the following results:

Table 4.3: Failure loads according to DIN 1052:2004-08

Geometry (a/H)	$P_{f,c}$ (kN)	$P_{f,v}$ (kN)
0,25	2087	3585
0.16	1391	2390
0.12	1043	1793
0.08	696	1195
0.06	522	896
0.04	348	598

4.1.3 Joint strength according to fracture mechanics

The joint strength according to LEFM, as calculated in chapter 3, can be seen in table 4.4.

4.2 Comparison and evaluation

In order to compare the results from *Linear Elastic Fracture Mechanics* (LEFM) to those from the *Glulam Handbook* (GmHk) and the *German Institute for Standardization* (DIN) the failure loads had to be calculated for the same material and geometry parameters.

Table 4.4: Failure load according to LEFM

Geometry (a/H)	P_f (kN)
0.25	1880
0.16	1505
0.12	1380
0.08	1109
0.06	1034
0.04	996

The values of $P_{f,LEFM}$ were obtained from diagram 3.3: for a known ratio of H/x_o the diagram yields the corresponding value of P_f/abf_v.
On the other hand, a and b are known geometry values and f_v is, in this case, given a value of 4 MPa

The results from applying the Glulam Handbook and the DIN standard are represented with two curves in the same figure respectively.

- A curve relating P_f to the compressive capacity of the notch is obtained from applying equation 4.1 (eq. 4.12 in the DIN) for various values of a (t_v in the DIN).

- A second curve was obtained by relating P_f to the shear capacity of the notch through equation 4.4.(eq. 4.16 in the DIN)

  (Both s in the Glulam Handbook and l_v in the DIN were obtained by using the upper limit of the shear stress distribution area, s=8a and l_v=8t_v respectively.)

The results are shown graphically in figure 4.3.
Some of the curves' coordinates are displayed in table 4.5.

Table 4.5: Comparison of failure loads

a, (t_v) (mm)	$P_{f,LEFM}$ (kN)	$P_{f,c,GH}$ (kN)	$P_{f,v,GH}$ (kN)	$P_{f,c,DIN}$ (kN)	$P_{f,v,DIN}$ (kN)
405	1263	2538	3136	2087	3585
260	792	1692	2091	1391	2390
194	621	1269	1568	1043	1793
130	479	846	1045	696	1195
97	455	634	784	522	896
65	407	423	523	348	598

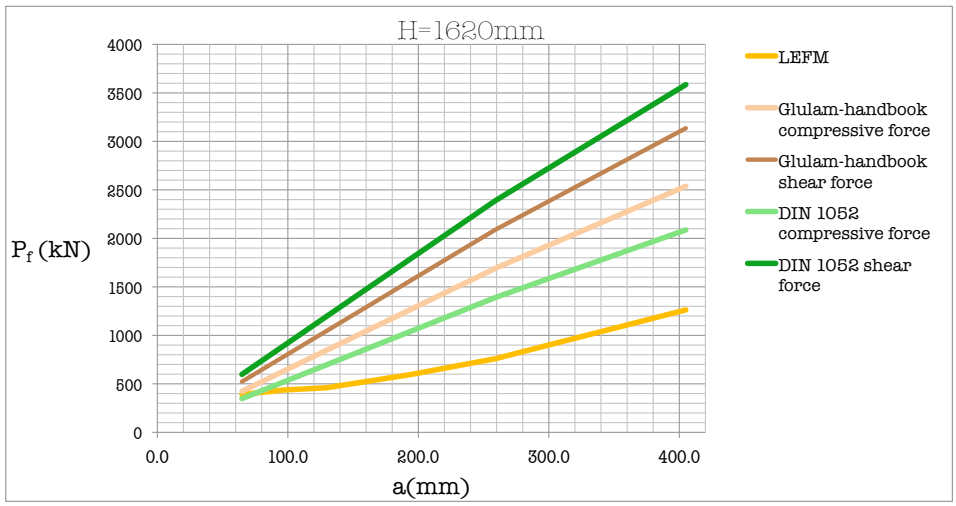

Figure 4.3: Comparison of failure loads for H=1620 mm

A second figure (fig. 4.4) is presented for a beam height of:
$H = 1620/4 = 405$ mm.

In this case the curves representing the results from the Glulam Handbook and DIN are proportionally modified only, as both calculating methods are independent of H.

The LEFM curve is obviously influenced by this new value of H: the H/x_o ratio is the first step to obtain a value of P_f and in this case a lower value of H implies a lower value of the ratio and thus a lower value of P_f for the same geometry and material values.

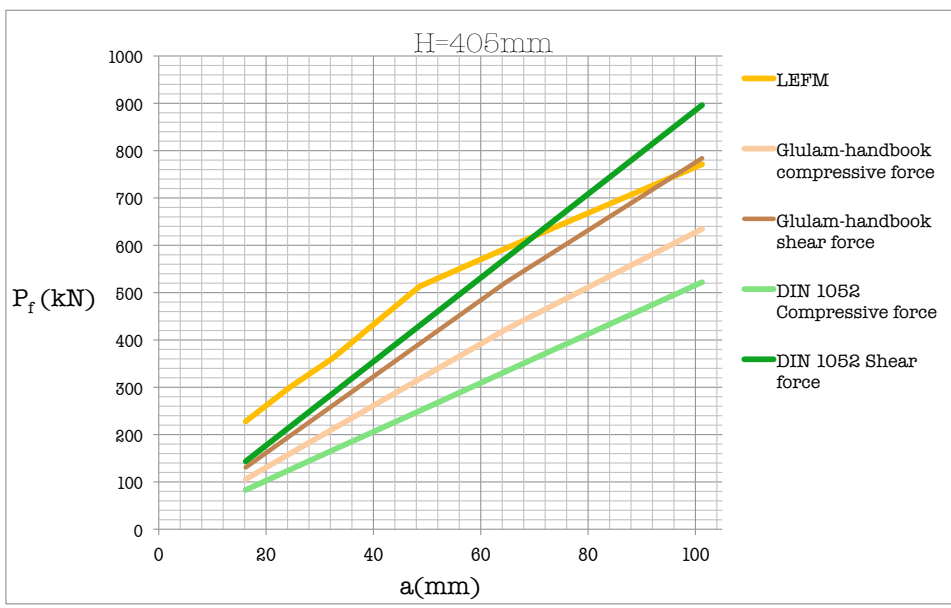

Figure 4.4: Comparison of failure loads for H=405 mm

Chapter 5

Conclusions

From examining the results presented in the previous chapter there are a few points that can be commented:

- *The failure load determined by the shear capacity, $P_{f,v}$, according to the DIN and the Glulam Handbook calculations, is greater than the failure load determined by the compressive capacity, $P_{f,c}$.*

  This is due to the fact that the values of s (l_v, DIN) used for the calculation were those of the upper limit of what the design method allowed ($s = 8a$, l_v=$8t_v$).

  This result implies surprising consequences because, as long as the designer chooses a long enough value of the shear stress distribution length, the shear capacity will never be the designing parameter of the notch.

  Both the Glulam Handbook and the DIN standard use the shear capacity only as a mechanism to ensure that a minimum shear stress distribution length is chosen.

- *The failure load, determined by the shear capacity according to the DIN standard, $P_{f,v,DIN}$, is always greater than according to the Glulam Handbook, $P_{f,v,GH}$.*

  The DIN standard uses the horisontal component of the compressive force in the strut F_H (see equation 4.11) while the Glulam Handbook uses the component that is perpendicular to the contact area, F_1 in figure 4.2. This can be understood as a more conservative approach by the Glulam Handbook compared to the DIN.

- *The failure load determined by the compressive capacity according to the Glulam Handbook , $P_{f,c,GH}$, is higher than according to the DIN standard, $P_{f,c,DIN}$.*

  This variation is due to the existing difference in the formula for calculating the off-axis uniaxial compressive strength of wood, $f_{c,\alpha}$ (equation 4.2 and

equation 4.9). Figure 5.1 shows the difference between the formulas to calculate material strengths at an angle to the grain provided by the DIN 1052 standard and the Glulam Handbook.
The DIN equation provides a more developed expression, including the shear strength parallel to the grain. This results in more conservative (safer) strength values than those obtained from the Glulam Handbook.

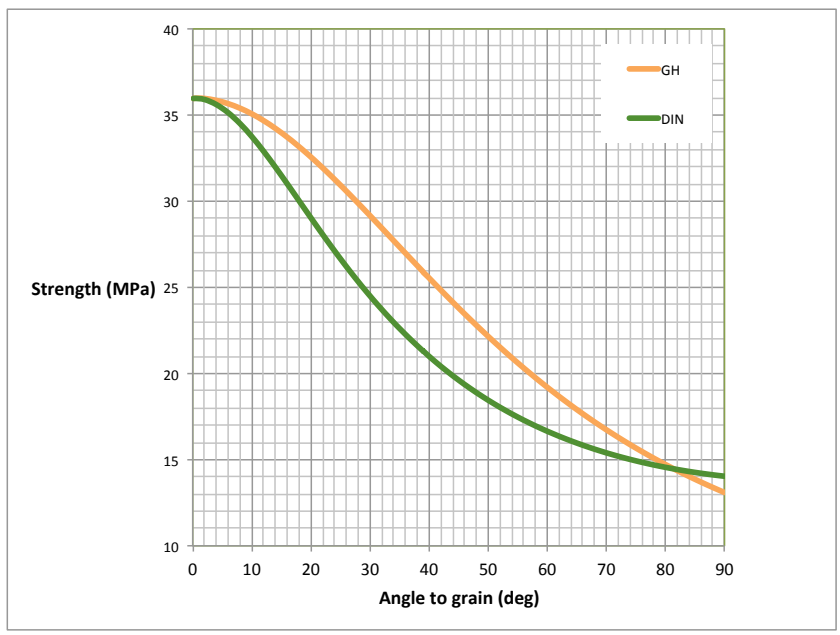

Figure 5.1: Comparison of strength variation with angle

- *The results obtained through Linear Elastic Fracture Mechanics ,LEFM, are lower than both design methods for a beam of great size. The opposite is true for a much lower beam.*
  This is a significant result as it clearly defines an important well-known phenomena with a very old history, namely the *size effect*.
  General *size effects* describe the dependency of strength on dimension whereby a loss of strength is assumed with increasing size.[17]
  Mechanical characteristics of structures, particular strength properties, are in general in connection with a reference dimension, which defines a material inherent dimension.

  Despite extensive empirical evidence, this phenomenon is still not taken into account in most specifications of the design codes for concrete structures, as well as the design practices for polymer composites, rock masses and timber.[14]
  However, some standards concerning construction timber incorporate size

effect considerations (eg. DIN 1052, EN 1995) in the form of *size factors.*[17]. These serve as strength increasing factors for structures and components with dimensions smaller than the reference case.

The present report highlights the fact that neither the DIN nor the Glulam Handbook consider any size effects for the design of haunches (*birdmouth* joints) and therefore exactly the same result is obtained for 2 greatly different geometries, see figures 4.3 and 4.4.

According to [15] it seems reasonable to expect even a greater difference between the results determined by the standard codes (DIN, GH) and those determined by the LEFM had the *size effect law* been taken into account when modelling the later.

5.1 Future Work

The results of this report point to several interesting directions for future work:

- When working with LEFM the size effects should be taken into account by using, for example, the size effect law defined in [16]. The latest results of investigations from [14] et. al should be taken into consideration in order to form a better understanding of the Size effect phenomena on timber, its consequences and its implications.
- A detailed comparison study of the formulae to determine the off-axis uniaxial strengths of timber. (Hankinson's as in [1] and the DIN standard 1052.)
- The calculation methods in this report need to be verified further by comparison to empirical results. Extensive lab tests would have provided a broader understanding of the behaviour of the haunch. The use of the mean stress method could then also be further verified against experimental data.

Bibliography

[1] Olle Carling et al. *Limträ Handbok.* Svenskt Limträ AB,Stockholm, 2001.

[2] *Snö och Vindlast 1997.* Boverket, 1997.

[3] *Boverkets Konstruktionsregler BKR, 2003.* Boverket, 2003.

[4] Gustafsson, P-J. *Mean stress aproach and initial crack aproach* RILEM TC/133, Lund University , Lund, 2002.

[5] http://www.glulam.co.uk

[6] Morris, V., Gustafsson, P-J. and Serrano, E. *The shear strength of lightweight beams with and without a hole-a preliminary study.* COST 508-Wood Mechanics Proc. of the 1995 Wood Mechanics Workshop on Mechanical Properties of Panel Products. Watford, UK, 1995.

[7] Sven Thelandersson, Hans J. Larsen. *Timber Engineering.* John Wiley & Sons, West Sussex, 2003.

[8] Jack A. Collins. *Failure of Materials in Mechanical Design:Analys, Prediction, Prevention, 2nd Ed..* Wiley Interscience, 2nd ed. September 7, 1993.

[9] Steve Lampman *Mechanics and mechanisms of fracture:an introduction.* ASM International, 1st ed. August, 2005.

[10] Rooke, D.P. and Cartwright, D.J. *Compendium of stress intensity factors.* HMSO Ministry of Defence. Procurement Executive. 1976.

[11] Anderson, T.L. *Fracture mechanics: fundamentals and applications.* CRC Press. 2005.

[12] Tada, Hiroshi; P. C. Paris; George Rankine Irwin. *The Stress Analysis of Cracks Handbook.* American Society of Mechanical Engineers. 3rd ed. February 2000.

[13] http://www.simulia.com/products/abaqus_cae.html

[14] Zdeněk P. Bažant. Arash Yavari. *Is the cause of size effect on structural strength fractal or energic-statistical?.* Engineering Fracture Mechanics. Volume 72, Issue 1. January 2005, Pages 1-31.

[15] S. Morel and G.Valentin. *Size effect in Crack Shear Strength of Wood.* Journal de physique IV. Colloque C6, supplémment au Journal De Physique III, Volume 6, octobre 1996.

[16] S. Morel and G.Valentin. *Effet d'echélle et résitance á la fissuration par cisaillemet du bois.* Actes du 30éme colloque annuel du Groupe Francais de Rhéologie, Bourdeaux, Volume XIV, N 1, pp 285-294. 1995.

[17] R.Brandner, T. Bogensperger G.Jeitler, G. Schickhofer. *Size effect considerations for linear structural elements of timber.* In the frame of COST E55-Modelling of the performance of timber structures.

[18] ABAQUS INC., ABAQUS getting started manual. Version 6.4. 2003

[19] http://www.lanik.com

[20] Michel Goossens, Sebastian Rahtz and Frank Mittelbach. *The LaTeX Graphics Companion.* Addison-Wesley, Reading, Massachusetts, 1997.